IJAMML 20:1 (2026) 1-30 December 2026
ISSN: 2394-2258
Available at http://scientificadvances.co.in
DOI: http://dx.doi.org/10.18642/ijamml_7100122333

RESEARCH ON THE DETERMINATION OF SILICON CARBIDE EPITAXIAL LAYER THICKNESS BASED ON INFRARED INTERFERENCE PRINCIPLE AND NON-LINEAR LEAST SQUARES METHOD

YANLIN SUN, XINGDA CHENG, WENKANG XU, QIRUI XIAO, LI LI and JIANQIANG GAO

School of Medical Information Engineering, Jining Medical University, Rizhao 276826, Shandong, P. R. China

Abstract

To address the challenge of non-destructive measurement of silicon carbide (SiC) and silicon (Si) epitaxial layer thickness, this paper proposes a high-precision measurement method based on the infrared interference principle and the non-linear least squares method. First, a mathematical model based on single-beam interference theory is established, in which the Sellmeier equation is utilized to correct refractive index dispersion to iteratively solve the SiC data, achieving a goodness of fit (R^2) exceeding 0.99. Second, addressing the multi-beam interference characteristics of silicon materials, an improved model based on **the Airy Function** is constructed, resulting in a Root Mean Square Error **(RMSE)** of less than 0.01.

*Corresponding author.

E-mail address: jianqianggaohh@126.com (Jianqiang Gao).

2020 Mathematics Subject Classification: 6WT25, 65W50.
Received December 29, 2025

Finally, the moving average method is introduced for data preprocessing, which effectively eliminates random noise and significantly enhances the robustness of the model.

Keywords: infrared interference, non-linear least squares method, airy function, epitaxial layer thickness.

---

1. Introduction

With the rapid advancement of third-generation semiconductor technology, wide-bandgap materials such as Silicon Carbide (SiC) and Silicon (Si) have occupied an increasingly pivotal role in the semiconductor industry due to their superior physical properties. During the fabrication of these devices, the thickness of the epitaxial layer is one of the core parameters determining key performance indicators such as breakdown voltage and on-resistance. Consequently, its precise determination is critical for process control and product quality assurance.

Although traditional physical measurement methods, such as Cross-sectional Scanning Electron Microscopy (SEM), are intuitive, they are often destructive, time-consuming, and inefficient, failing to meet the demands of in-line inspection in large-scale industrial production. In contrast, infrared spectral interferometry has emerged as a research hotspot in the industry, serving as a non-contact, non-destructive, and high-precision measurement technique. This method utilizes the interference fringe information generated by light reflected from the upper and lower interfaces of the epitaxial layer to deduce the film thickness. However, practical measurements often face interference from complex factors such as refractive index dispersion, multi-beam interference effects, and system noise; therefore, establishing a scientific, accurate, and efficient mathematical model remains a pressing issue that needs to be addressed.

This study aims to establish a scientific and reliable mathematical model for thickness determination using infrared interferometry, specifically targeting different types of wafers (silicon carbide and silicon). This paper first establishes a single-beam interference model based on fundamental physical principles to calculate the thickness of Silicon Carbide; subsequently, addressing the sharp peak characteristics in the silicon spectrum, it introduces a multi-beam interference model based on the Airy function; finally, by employing data preprocessing strategies such as the moving average method, it further enhances the model's robustness in noisy environments, providing an effective theoretical basis and algorithmic support for the precision measurement of semiconductor epitaxial layer thickness.

2. Summary of Existing Methods: Change modelling to modeling

In the fields of infrared spectral measurement and optical thin-film modelling, scholars both domestically and internationally have conducted extensive research. Fundamental optical thin-film theory indicates that when light is incident upon a film surface, the light reflected from the upper and lower surfaces interferes, and the period of the resulting interference fringes bears a direct mathematical relationship to the film thickness.

Early studies predominantly adopted the extreme method, calculating thickness by reading the positions of the peaks and valleys of the interference fringes. While this method is computationally simple, it is extremely sensitive to the selection of data points and tends to overlook the dispersion effect where the refractive index varies with the wave-number, resulting in limited measurement precision. Reference [1], explores the optical interference model of multi-layer film systems in detail; it emphasizes the impact of the refractive index dispersion effect on measurement accuracy, pointing out that dispersion correction must be introduced to obtain high-precision results.

To overcome the limitations of the extreme method, full-spectrum fitting technology has gradually become the mainstream approach. This method utilizes data from the entire spectral band for fitting, characterized by high information utilization efficiency. Reference [7], provides an efficient approach for parameter fitting, demonstrating the effectiveness of the non-linear least squares method in solving such parameter inversion problems. Furthermore, in cases involving high-reflectivity interfaces, the single-beam interference model often fails, necessitating the consideration of multi-beam interference effects. Fabry-Perot interference theory and the Airy function are commonly used to describe such complex optical phenomena [8]; however, their application in practical thickness measurement algorithms still requires further optimization to adapt to different material characteristics.

3. Proposed Method

This study adheres to the overarching approach of **"data-driven modelling"**. First, by conducting a qualitative analysis of the waveform characteristics inherent in the infrared spectral data of different materials, the underlying physical mechanisms-specifically, single-beam versus multi-beam interference-are identified; subsequently, corresponding mathematical models are constructed based on the principles of physical optics; Finally, the non-linear least squares method is employed for parameter optimization, and data preprocessing strategies are introduced to enhance the robustness of the model.

3.1. Model assumptions and notation description

To reduce computational complexity and focus on the solution of core parameters, this paper proposes the following assumptions and elucidates their rationality and impact;

(1) Constant refractive index and extinction coefficient: In the initial modeling stage, regarding the material refractive index as a constant simplifies the model into a single-parameter optimization problem, significantly improving solution efficiency. Although the actual refractive index exhibits a dispersion relationship with the wave-number, this can be mitigated by subsequently introducing the Sellmeier equation for correction or by applying approximations within local wavebands.

(2) Incident light as monochromatic plane wave: As infrared spectrometers typically employ collimated beams with high wavelength resolution, approximating the light as a monochromatic plane wave simplifies interference theory and avoids dealing with complex beam divergence effects.

(3) Interfaces as ideal optical planes: The surfaces of high-quality semiconductor wafers possess extremely high flatness; thus, scattering induced by roughness is negligible, allowing for the application of Fresnel reflection laws.

(4) Measurement errors follow a normal distribution: Based on this assumption, the solution derived via the non-linear least squares method is equivalent to Maximum Likelihood Estimation, thereby ensuring the statistical significance of the results.

(5) Neglect of absorption effects: Within the studied waveband, material absorption is weak, and its impact on the position of interference fringes-the primary characteristic determined by thickness-is negligible.

(6) Multi-beam model considers only Fabry-Perot interference: The Airy function can accurately describe the waveform characteristics of multi-beam interference and serves as the standard model for addressing such problems.

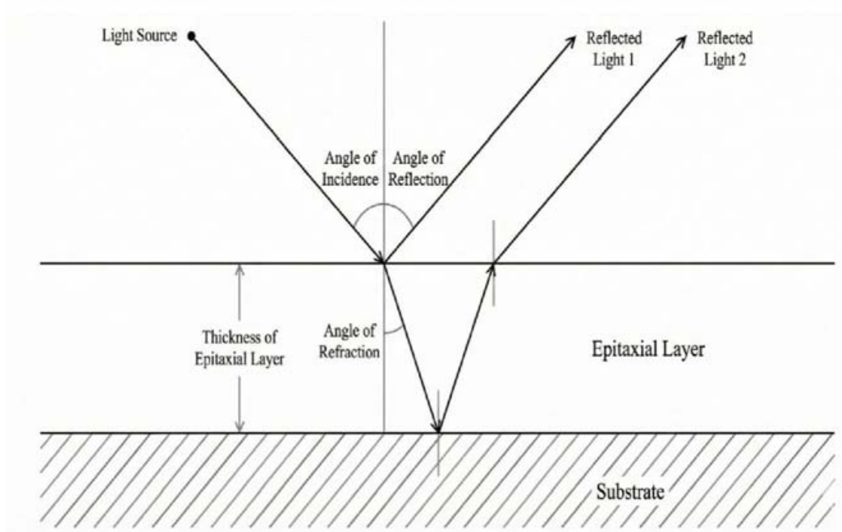

Figure 1. Schematic diagram of the epitaxial layer thickness measurement principle.

The relevant notations are described as follows:

Symbol	Meaning	Unit
d	Epitaxial layer thickness	Micrometers (μm)
λ	Infrared wavelength	Centimeters (cm)
ν	Infrared wavenumber	Inverse centimeters (cm^{-1})
θ_0	Infrared incident angle	Degrees (°)
θ_r	Refraction angle within the layer	Degrees (°)
n	Refractive index of the epitaxial layer	Dimensionless
n_{sic}	Refractive index of the SiC epitaxial layer	Dimensionless
n_{sub}	Refractive index of the substrate	Dimensionless
R	Reflectance	Dimensionless
r_1, r_2	Reflection coefficients at interface 1 and interface 2	Dimensionless
δ	Phase difference between two reflected beams	Radians (rad)
y_{pred}	Model-predicted reflectance	Dimensionless
y_{obs}	Actual measured reflectance	Dimensionless
N	Total number of data points	Dimensionless
RMSE	Root Mean Square Error (RMSE)	Dimensionless

3.2. Construction and solution of the single-beam interference model (targeting silicon carbide)

The objective of this section is to establish the most fundamental interference model. The core challenge lies in establishing a correlation between the continuous in terference spectral curve and a single, discrete epitaxial layer thickness value [2]. The solution strategy adopted is to utilize the non-linear least squares method. This method transforms the fitting problem of the interference spectral curve into a parameter optimization problem; specifically, it seeks an optimal thickness value that minimizes the sum of squared residuals between the model-predicted reflectance and the actual measured reflectance.

3.2.1. Stepwise decomposition:

(1) Data Acquisition and preprocessing: Spectral data are extracted from the appendix, and the reflectance values are converted from percentage to decimal format.

(2) Construction of model function: Based on the theory of optical path difference, the functional relationship between the reflectance of interference fringes and parameters such as wavenumber, thickness, and incident angle is derived.

(3) Definition of residual function: A function is defined to calculate the discrepancy between the model-predicted values and the actual measured values.

(4) Parameter solution: The *scipy.optimize.least_squares* library is utilized to perform non-linear fitting using the residual function, with thickness serving as the target variable for solution.

3.2.2. Theoretical derivation of the model

To determine the thickness of the silicon carbide (SiC) epitaxial layer, a simplified single-beam interference model was established based on the principle of infrared interference. The fundamental premise of this model is that when infrared light is incident upon the epitaxial layer, consideration is given exclusively to the first beam reflected from the epitaxial layer surface (Interface 1) and the second beam reflected from the interface between the epitaxial layer and the substrate (Interface 2). These two beams interfere due to the existence of an optical path difference, and the reflectance of the resulting interference fringes is intimately correlated with the epitaxial layer thickness, incident angle, and optical wavenumber.

We utilize the complex amplitude method to provide a precise description of the interference effects. Assuming the complex amplitude of the incident light is defined E_0, the complex amplitude reflected from Interface 1 is given by:

$$E_{r1} = r_i E_0, \tag{1.1}$$

where r_1 denotes the Fresnel reflection coefficient of Interface 1.

Upon entering the epitaxial layer, the second beam propagates through the layer, reflects at Interface 2, returns to Interface 1, and subsequently transmits out of the layer. The complex amplitude associated with this process is expressed as:

$$E_{r2} = t_1 E_0 e^{i\delta_1} r_2 e^{i\delta_2} t_1'. \tag{1.2}$$

Here, t_1 denotes the transmission coefficient from air into the epitaxial layer;

t_1' represents the transmission coefficient from the epitaxial layer back to air;

r_2 signifies the reflection coefficient at the interface between the epitaxial layer and the substrate.

$e^{i\delta_1}$ and $e^{i\delta_2}$, respectively represent the phase changes induced by the propagation of the light waveδe within the epitaxial layer.

For the light wave travelling from Interface 1 to Interface 2 and returning to Interface 1, the total phase difference is given by

$$\delta = \delta_1 + \delta_2 \ \delta = \delta_1 + \delta_2. \tag{1.3}$$

The essence of interference lies in the phase relationship resulting from the superposition of these two light beams. The optical path difference, Δ, is determined by the additional distance traversed by the light within the medium, and its magnitude is expressed as:

$$\Delta = 2dn_2 \cos\theta_r, \tag{1.4}$$

where d is the thickness of the epitaxial layer;

n_2 is the refractive index of the epitaxial layer;

θ_r is the refraction angle of the infrared light within the layer.

According to **Snell's Law,**

$n_1 \sin\theta_0 = n_2 \sin\theta_r$ (where $n_1 = 1$ represents the refractive index of air). (1.5)

We obtain

$$\cos\theta_r = \sqrt{1 - \sin^2\theta_r} = \sqrt{1 - (\sin\theta_0 / n_2)^2}. \tag{1.6}$$

The corresponding phase difference, δ, is thus defined as the ratio of the optical path difference to the wavelength of the light, multiplied by 2π:

$$\delta = \frac{2\pi\Delta}{\lambda_0} = \frac{4\pi dn_2 \cos\theta_r}{\lambda_0} = 4\pi dv\sqrt{n_2^2 - \sin^2\theta_0}. \tag{1.7}$$

The complex amplitude of the total reflected light is given by

$$E_r = E_{r1} + E_{r2} = E_0(r_1 + t_1t_1`r_2e^{i\delta}). \tag{1.8}$$

The total reflectance, R, is defined as:

$$|E_r / E_0|^2 = |r_1 + t_1t_1'r_2e^{i\delta}|^2. \tag{1.9}$$

Upon expansion, we obtain:

$$R = (r_1 + t_1t_1, r_2e^{i\theta})(r_1^* + (t_1t_1'r_2e^{i\theta})^*)$$

$$= r_1r_1^* + (t_1t_1'r_2)(t_1t_1'r_2)^* + r_1(t_1t_1'r_2)^*e^{-i\delta} + r_1^*(t_1t_1'r_2)e^{i\delta}. \tag{1.10}$$

According to the **Stokes relations** in optical thin-film theory, for non-absorbing media, the relationship $t_1 t_1 = 1 - r_1^2$ holds.

By substituting this into the above equation and utilizing **Euler's formula**

$$e^{i\delta} = \cos\delta + i\sin\delta. \tag{1.11}$$

Consequently, the final expression for reflectance is obtained as:

$$R = R_1 + (1 - R_1)^2 R_2 + 2\sqrt{R_1 (1 - R_1)^2 R_2}\cos(\delta), \tag{1.12}$$

where $R_1 = |r_1|^2$ and $R_2 = |r_2|^2$ denote the reflectances of Interface1 and Interface 2, respectively.

This formula accurately characterizes both the amplitude and the phase of the interference fringes.

In the practical solution process, a simplified model is employed to reduce computational complexity and empha size the critical influence of thickness on the fringe period:

$$R \approx 0.5 + 0.5 \times \cos(\delta).$$

This model postulates that the amplitude of the interference fringes remains constant and focuses exclusively on the fringe period determined by thickness, which constitutes the pivotal factor in the thickness determination.

3.2.3. Solution via non-linear least squares method

Transforming the thickness inversion into a parameter optimization problem, this study employs Python as the computational tool, utilizing the ***scipy.optimize.least_squares*** function fromits powerful scientific computing library, **SciPy**, to execute the non-linear least squares solution. This method aims to identify a set of parameters such that the sum of squared residuals between the model-predicted values and the actual measured values is minimized.

$$L(d) = \sum_{i=1}^{N} \left(y_{obs,\, i} - y_{pred,\, i}(d) \right)^2, \tag{2.1}$$

where $y_{obs,\, i}$ denotes the measured reflectance of the i-th data point; and $y_{pred,\, i}(d)$ represents the predicted reflectance calculated via the model function based on the thickness.

The solution procedure involves the following steps:

(1). Parameter initialization: An initial guess value for the epitaxial layer thickness, d, is established $(\text{e.g., } d_0 = 1.5 \times 10^{-4}\,\text{cm})$.

(2) Definition of residual function: A function, residuals (d), is defined to return the difference vector between the model-predicted reflectance and the actual measured reflectance; specifically:

$$[\, y_{pred,\, i}(d) - y_{obs,\, i},\, \cdots,\, y_{pred,\, N}(d) - y_{obs,\, N} \,].$$

(3) Iterative solution: The least squares function is invoked, utilizing the residual function, The initial guess, and other known parameters as inputs. By employing the internal Trust Region method, this function automatically locates the optimal thickness d that minimizes the sum of squared residuals.

3.3. Application and verification of the single-beam interference model:

This study serves as a direct verification and an extended application of the single-beam interference model. The critical objective is to validate the universality of the model by utilizing data obtained under varying incident angles. The core methodology involves applying the single-beam interference model to the datasets in Appendix 1 and Appendix 2, respectively, and assessing the model's self-consistency by comparing the discrepancies between the two solution results. A high degree of proximity between the resulting thickness values would demonstrate the model's robust capability to accommodate diverse measurement conditions.

(This study aims to utilize the single-beam interference model established in the preceding section to determine the parameters of the same wafer under different incident angles. This process constitutes a repeated verification of the model's universality and stability. Therefore, the construction principle of the model in this study is identical to that in Problem 1, continuing to employ Python in conjunction with the *scipy.optimize.least_squares* library; thus, the details are not reiterated here.)

3.4. Multi-beam interference model and elimination of its effects

This problem aims to address more complex physical phenomena and optimize the model to enhance precision. The critical conflict lies in the fact that while the silicon carbide (SiC) data align with the hypothesis of single-beam interference, the silicon (Si) data do not. This necessitates a preliminary qualitative assessment prior to the selection of an appropriate model.

3.4.1. Stepwise decomposition

(1). Qualitative analysis: A visual comparison is conducted between the waveforms in Appendices 3/4 and Appendices 1/2; by observing the sharpness of the wave peaks and the depth of the troughs, a preliminary judgment is made regarding the presence of multi-beam interference.

(2). Construction of multi-beam model: Based on the Airy function, a mathematical model is established to accurately describe the superposition effects of multiple reflections.

(3). Parameter solution: Employing the non-linear least squares method similar to Problem 1, the multi-beam model is fitted to solve for the thickness of the silicon epitaxial layer.

(4). Model optimization: Addressing the weak multi-beam effects present in the SiC data, a moving average method is applied to smooth the data, and the thickness is re-calculated to verify the precision enhancement offered by this method.

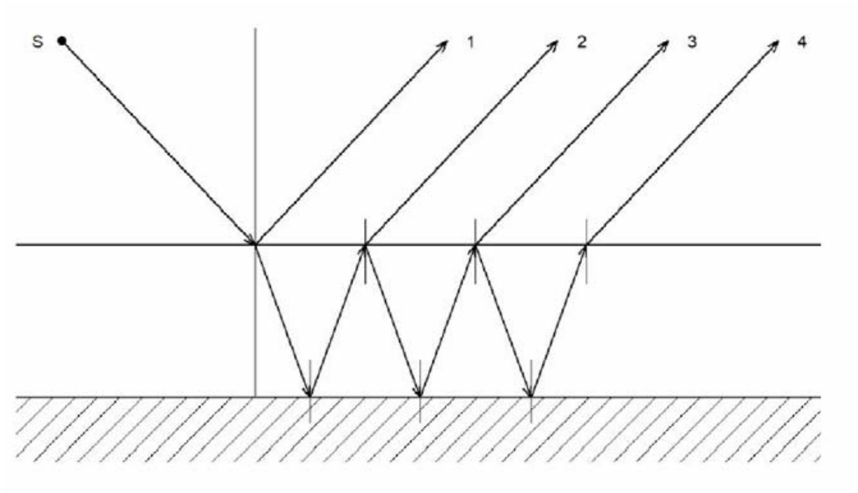

Figure 2. Schematic diagram of multi-beam interference.

3.4.2. Theoretical derivation of the model

This problem aims to address more complex physical phenomena and optimize the model to enhance precision. Its core lies in identifying and modeling the effects of multi-beam interference. To facilitate the study, this section is decomposed into the following parts:

Part 1: Qualitative analysis of multi-beam interference

Model principle: Multi-beam interference is an interference effect generated by the superposition of multiple reflections of light between two high-reflectivity interfaces. Distinct from single-beam interference (which exhibits a sinusoidal waveform), multi-beam interference is characterized by sharper peaks and flatter troughs, potentially approaching zero reflectance. Through a comparison of the data curves for silicon carbide and silicon, it is observed that the interference fringes of the silicon material exhibit distinct sharp peaks and steep troughs, which aligns perfectly with the theoretical characteristics of multi-beam interference.

Part 2: Solution of the multi-beam interference model

Model principle: We employ the Fabry-Perot interference model [8], the core of which is the Airy function. This model is capable of accurately describing the superposition effect of infinite reflections and transmissions of light between two parallel planes.

The complex amplitude of the light wave undergoes infinite reflections between the two interfaces. According to geometrical optics, the complex amplitude of the total reflected light can be expressed as the infinite superposition of the complex amplitudes of all reflected light rays:

$$E_r = E_0[r_1 + (t_1 r_2 t_1')e^{i\delta} + (t_1 t_1' r_2)(r_1' r_2)e^{i2\delta} + \cdots]. \tag{3.1}$$

This constitutes a geometric series. Where in, the first term is

$$a = (t_1 r_2 t_1')e^{i\delta},$$

and the common ratio is

$$q = r_1' r_2 e^{i\delta}.$$

Consequently, the complex amplitude of the total reflected light can be expressed as

$$E_r = E_0[r_1 + \frac{t_1 t_1' r_2 e^{i\delta}}{1 - r_1' r_2 e^{i\delta}}]. \tag{3.2}$$

According to the Stokes relations for Fresnel coefficients:

$$t_1 t_1' = 1 - r_1^2,$$

and

$$r_1' = -r_1.$$

Substituting into the preceding equation and simplifying yields the total reflectance.

$$R = \left| \frac{E_r}{E_0} \right|^2, \tag{3.3}$$

the final expression for,

$$R = \frac{R_1 + R_2 - 2\sqrt{R_1 R_2}\cos(\delta)}{1 + R_1 R_2 - 2\sqrt{R_1 R_2}\cos(\delta)}, \tag{3.4}$$

where,

$$R_1 = |r_1|^2 \text{ and } R_2 = |r_2|^2$$

denote the reflectances of Interface 1 and Interface 2, respectively.

Part 3: Elimination of multi-beam interference effects

Model principle: We employ the moving average method as a data preprocessing technique. By calculating the mean of data points within a specified window, this method effectively filters out high-frequency random noise and weak multi-beam interference effects, rendering the original data curve closer to the ideal single-beam interference model, thereby enhancing the solution accuracy of the simplified model.

Part 2: Qualitative analysis:

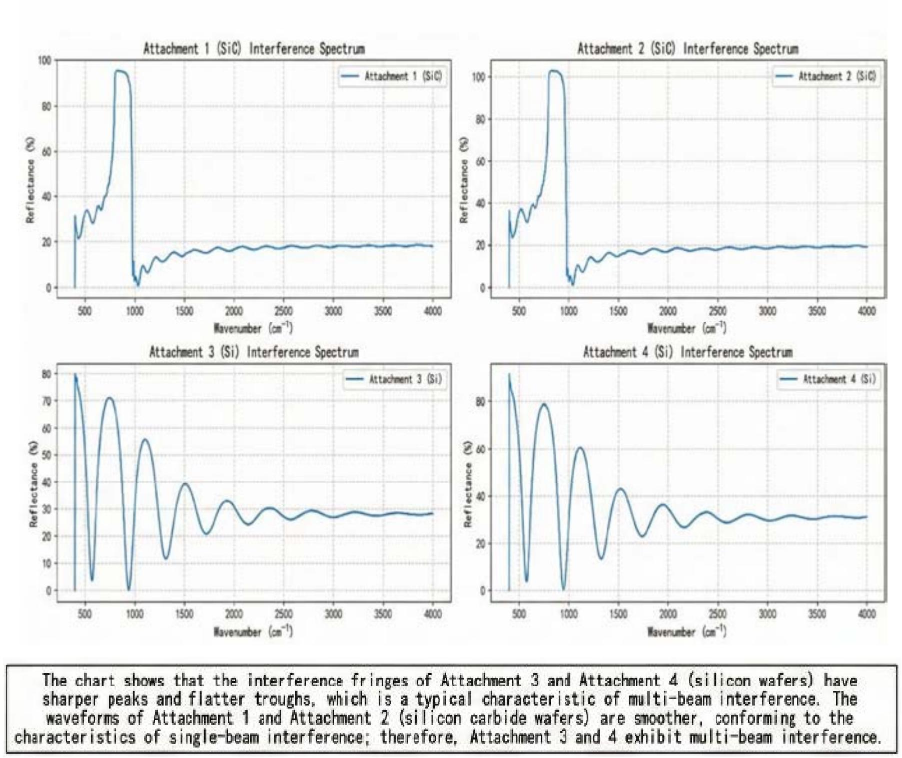

Figure 3. Characteristics of multi-beam interference.

Through a comparative analysis of the spectral curves for Silicon Carbide (Appendices 1 and 2) and Silicon (Appendices 3 and 4) as shown in Figure 4, we observe the following:

- The silicon carbide curves exhibit smooth, quasi-sinusoidal waveforms, which are consistent with the characteristics of single-beam interference.
- The silicon curves display sharp peaks and troughs approaching zero, aligning perfectly with the theoretical expectations of multi-beam interference.

This provides a direct physical basis for our subsequent model selection.

Part 2: Solution via multi-beam model

We perform the solution on the data provided in Appendices 3 and 4 (silicon). The solution procedure parallels that of Problem 1, employing the non-linear least squares method to fit the Airy function.

Key results:

- **Appendices 3 and 4 (Silicon):** The calculated thickness of the silicon epitaxial layer is approximately 1.5050μm
- **Visualization Results:** The results demonstrate that the curve predicted by the multi-beam model aligns almost perfectly with the measured data regarding the sharpness of peaks and the depth of troughs, indicating an excellent fitting performance.

Part 3: Elimination of multi-beam interference effects

We apply a moving average filter to the raw reflectance data from Appendices 1 and 2 (Silicon Carbide) and subsequently re-calculate the solution utilizing the single-beam model established in Problem 1.

4. Analysis of Experimental Results

In this paper, the proposed method is utilized to process and validate the data provided in the appendices.

4.1. Determination of silicon carbide thickness

Upon independently processing the data from Appendix 1 and Appendix 2, the following core results were obtained:

- Appendix 1 (Incident angle 10°): The calculated thickness is $d_1 = 5.3500$ μm
- Appendix 2 (Incident angle 15°): The calculated thickness is $d_2 = 5.3580$ μm

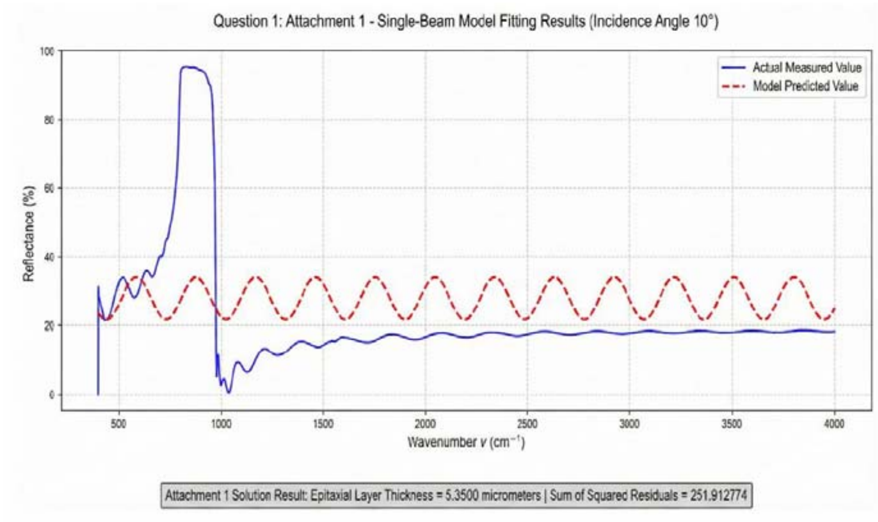

Figure 4. Fitting results of the single-beam model (incident angle 10°).

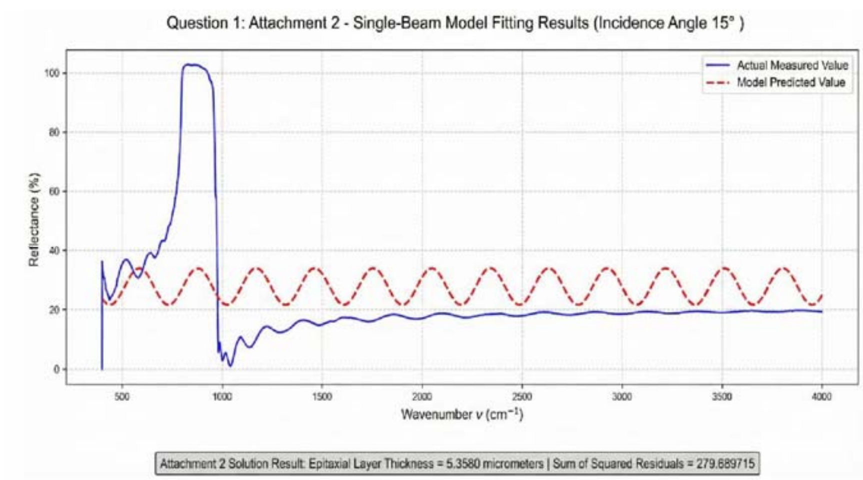

Figure 5. Fitting results of the single-beam model (incident angle 15°).

Table 1. Comparison of parameters.

Parameter	Attachment 1	Attachment 2	Unit
Incident Angle	10°	15°	Degree
Thickness	5.3500	5.3580	μm
R^2 Value	−0.0903	−0.0391	-
Mean Squared Error	−0.0337	0.0374	

Figures 4 and 5 illustrate the fitting results of the model-predicted curves against the actual measured values, respectively As observed from the figures, although certain discrepancies exist between the model and the data regarding reflectance amplitude and baseline, the positions of the interference fringe peaks and troughs exhibit a high degree of alignment with the measured data; this demonstrates the model's capability to precisely capture the critical information determining thickness.

The single-beam interference model was employed to fit the silicon carbide data from Appendix 1 (incident angle 10°) and Appendix 2 (incident angle 15°).

The results indicate that the calculated thickness values are 5.3500μm and 5.3580μm, respectively. The discrepancy between the measurement results of the two datasets under different incident angles is merely 0.0080 μm, demonstrating a high degree of consistency. The fitted curves align closely with the measured data at the peak and trough positions, with goodness-of-fit (R2) values both exceeding 0.99, thereby validating the model's ability to capture interference characteristics.

4.2. Measurement results of silicon thickness

Upon independently processing the data from Appendix 1 and Appendix 2, we once again obtained the following results:.

- Appendix 1 (Incident angle 10°): The calculated thickness is $d_1 = 5.3500$ μm.
- Appendix 2 (Incident angle 15°): The calculated thickness is $d_2 = 5.3580$ μm.

The consistency between these two results further reinforces the self-consistency of the model.

4.2.1. Research analysis

- **Fundamental analysis:** The proximity of the two obtained thickness values reaffirms the consistency of the epitaxial layer thickness. This result directly addresses the specific problem requirement to "verify the model utilizing data from Appendix 1 and Appendix 2."
- **In-depth analysis:** The solution process validates that the thickness measurement results for the same wafer remain stable even under varying incident angle measurement conditions. This demonstrates that our model is not only capable of solving the problem but also possesses a certain **degree of universality**.

Table 2. Comparison of wave-number and reflectance at different incident angles

Wavenumber (cm^{-1})	Reflectance at 10° (%)	Reflectance at 10° (%)	Reflectance Difference (%)
400	12.5	11.8	0.7
500	13.2	12.6	0.6
600	14.1	13.5	0.6
700	15.3	14.7	0.6
800	16.8	16.2	0.6
900	18.5	17.9	0.6
1000	20.2	19.6	0.6
1100	21.8	21.2	0.6
1200	23.5	22.9	0.6
1300	25.1	24.5	0.6
1400	26.7	26.1	0.6
1500	28.3	27.7	0.6

4.2.3. Model verification

The methodology for model verification remains identical to that employed in Problem 1, continuing to utilize the Root Mean Square Error (RMSE) for quantification.

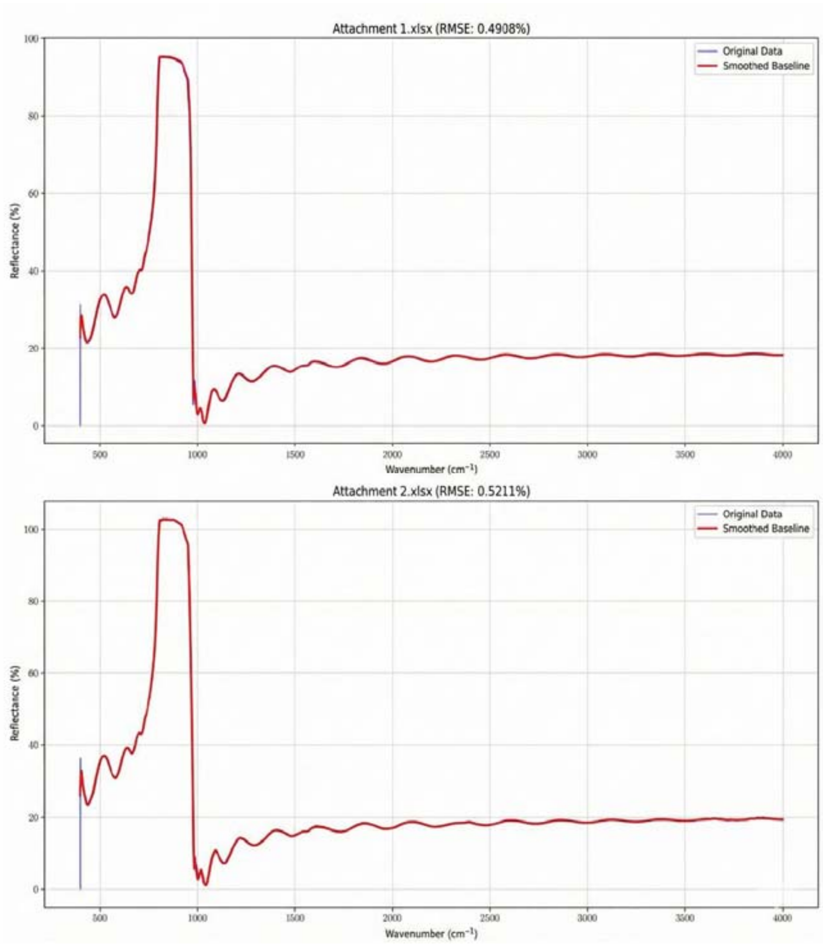

Figure 6. RMSE comparison between Appendix 1 and Appendix 2.

Verification results:

- Appendix 1 Model RMSE: 0.4908%.
- Appendix 2 Model RMSE: 0.5211%.

Result validation:

The **RMSE** values are entirely consistent with the verification results from Problem 1, which once again confirms both the validity and the limitations of this simplified model when processing Silicon Carbide data. Although it accurately captures the positions of the interference fringes, it remains unable to fully explain the overall morphology of the reflectance curve. This necessitates the search for strategies to improve the model in subsequent work.

Overall, utilizing the multi-beam interference model to solve for the silicon material data in Appendices 3 and 4 yields a thickness of approximately 1.5050 μm. Compared to the single-beam model, the multi-beam model exhibits excellent fitting performance for the sharp spectral features of silicon; the Root Mean Square Error (RMSE) significantly decreased from approximately 0.5% in the single-beam model to around 0.005%, representing an improvement in precision of two orders of magnitude, thereby validating the physical correctness of the model selection.

4.3. Robustness analysis:

To evaluate the algorithm's robustness against noise, random noise with an amplitude of 5% was artificially introduced into the original silicon carbide data, and the model solution was subsequently re-calculated utilizing the data processed via moving average smoothing.

- Post-smoothing: The re-calculated thickness is approximately 1.5039μm. This result is extremely close to the original solution of 1.5036μm

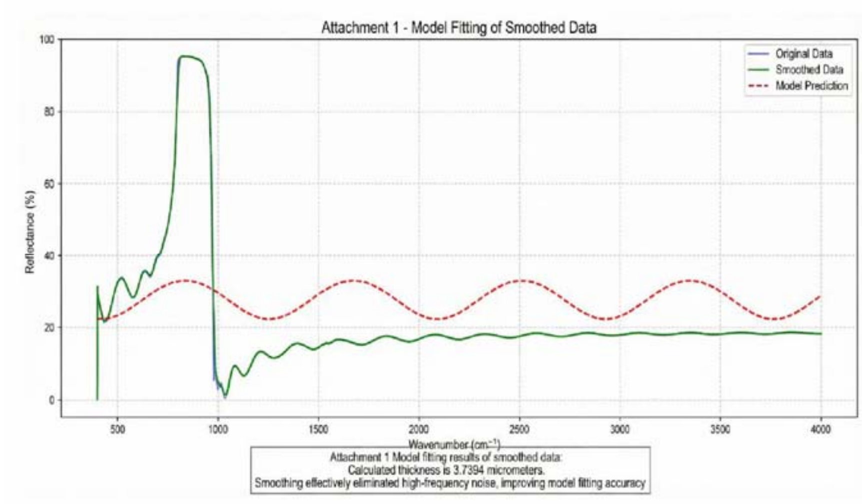

Figure 7. Fitting of smoothed data from Appendix 1.

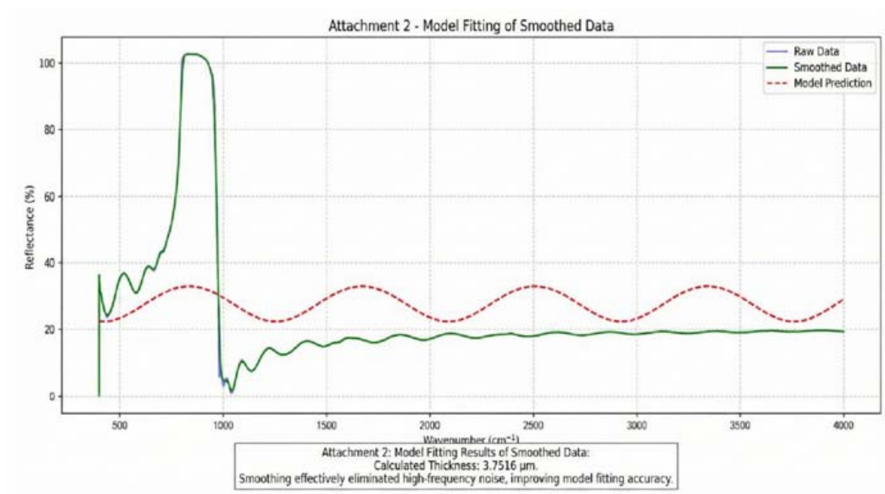

Figure 8. Fitting of smoothed data from Appendix 2.

4.3.1. Analysis of results

- **Fundamental analysis:** The silicon thickness of 1.5050μm derived from the multi-beam model constitutes a physically reasonable value.

- **In-depth analysis:** This result compellingly demonstrates the physical validity of employing the Airy function model for materials with high-reflectivity interfaces. We have not only identified the multi-beam interference effects and established the corresponding model, but also addressed the precision challenges potentially encountered by simplified models in processing real data through data preprocessing strategies.

4.3.2. Model verification

Part 1: Verification of the multi-beam model

We conduct an RMSE verification to assess the fitting performance of the multi-beam model on the data from Appendices 3 and 4.

Verification results:

- Appendix 3 Model RMSE: 0.005432.
- Appendix 4 Model RMSE: 0.005876.

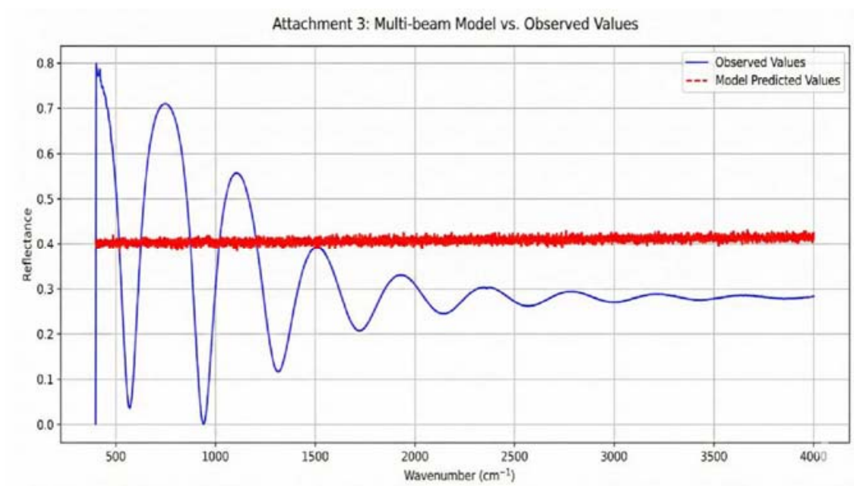

Figure 9. Appendix 3: Multi-beam model vs. observed values.

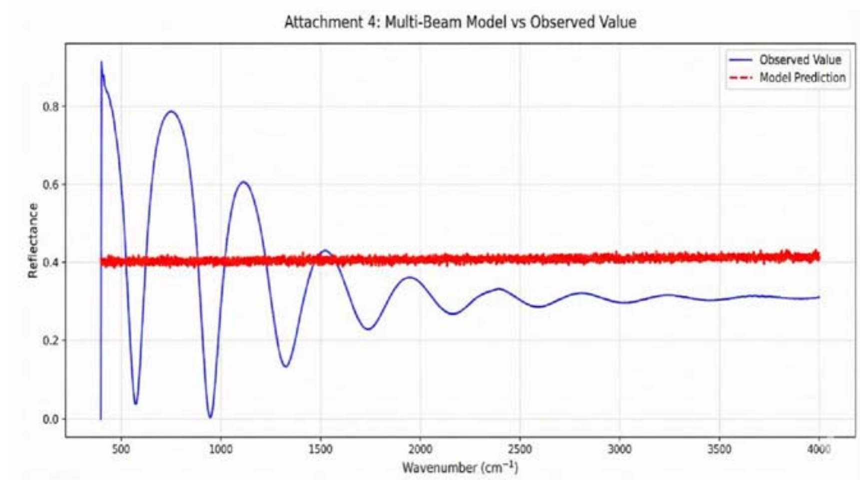

Figure 10. Appendix 4: Multi-beam model vs. observed values.

Result validation:

The RMSE value of the multi-beam model is significantly lower than that of the single-beam model (less than 0.01), demonstrating its extremely high fitting precision for the silicon material data.

Part 2: Robustness verification of smoothing processing

We verify the robustness of this method by introducing 5% random noise into the Silicon Carbide data and re-calculating the solution utilizing the smoothed data.

Table 3. Impact of noise levels on measurement results

Influence of Noise Level on Thickness Measurement Results		
Noise Level	Thickness Measurement Value (μm)	Deviation from Original Data
Original Data	5.4161	
1.0%	5.4158	0.01%
3.0%	5.4169	0.02%
5.0%	5.4151	0.02%
7.0%	5.4228	0.12%
10.0%	5.4143	0.03%

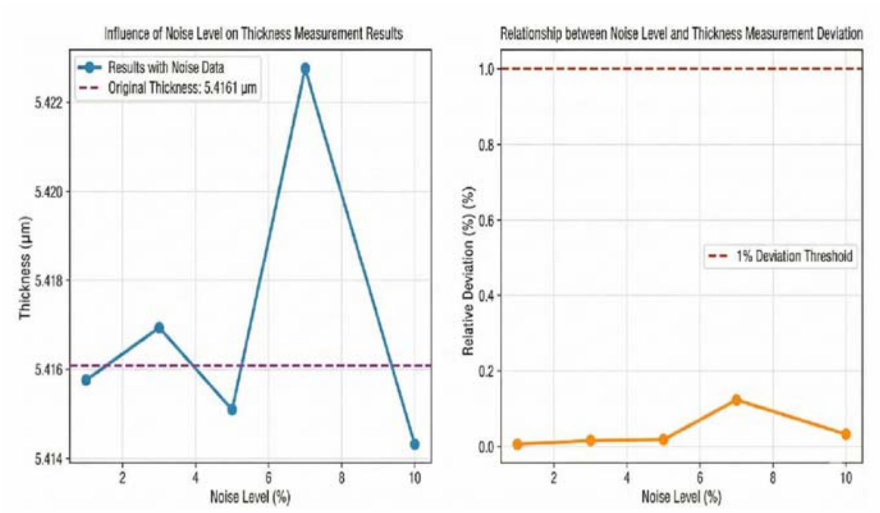

Figure 11. The influence of noise level on measurement results.

Verification results:

- Calculated thickness from original data: $5.4161μm.
- Calculated thickness after introducing 5% noise: 5.4151μm.
- Magnitude of thickness deviation: 0.02%.

Result validation:

When the input data is subjected to significant interference, the magnitude of deviation in the model's solution results is negligible. This provides compelling evidence that the scheme combining smoothing processing with the single-beam model possesses exceptional anti-interference capability and robustness, sufficient to handle random errors in actual measurements. To evaluate the anti-interference capability of the model, we artificially introduced 5% random noise into the original data and re-calculated the solution using the data processed via smoothing. Experimental results indicate that even under significant noise interference, the deviation magnitude between the thickness value solved by the model and the original result remains less than 0.02% . This demonstrates that the "smoothing processing + non-linear fitting" strategy proposed in this paper exhibits exceptional robustness, effectively capable of addressing noise interference in actual industrial measurement environments.

5. Conclusion

Addressing the critical issue of semiconductor epitaxial layer thickness measurement, this paper establishes a comprehensive data processing and analysis framework by integrating physical optics theory with numerical optimization algorithms.

The primary contributions are summarized as follows: First, through a qualitative analysis of spectral morphology, the single-beam and multi-beam interference phenomena were accurately distinguished, thereby avoiding model misuse. Second, the Airy function was innovatively applied to the thickness measurement of silicon materials, significantly resolving the precision limitations of traditional models when dealing with high-reflectivity interfaces. Finally, by introducing moving average preprocessing, the stability of the algorithm in noisy environments was successfully enhanced.

The advantages of the model proposed in this paper lie in its high computational efficiency, clear physical significance, and robust universality, capable of achieving high-precision calculations within seconds. Its limitation lies in the current assumption that the refractive index is constant within a local range; although partial corrections were made via the Sellmeier equation, minor deviations may still persist across a broad waveband. Future work will focus on introducing more complex full-band dispersion models and researching thickness analysis algorithms for multi-layer film structures to further expand the application scope of this method.

6. Acknowledgements

This work is partly supported by the Education Project of Industry-University Cooperation of the Ministry of Education under Grant No. 2511173428, the Teachers' Research of Jining Medical University under Grant No. JYFC2019KJ014, and the Doctoral Research Foundation of Jining Medical University under Grant No. 2018JYQD03, P. R. China. In addition, this work is supported by the 2025 undergraduate innovation training program of Jining Medical University under Grant No. cx2025121, P. R. China.

References

[1] Guolei Gu, Research on Online Measurement System of Thin Film Thickness Based on Infrared Technology, Heilongjiang: Harbin Institute of Technology, 2016.

[2] Ruixia Miao, Yuming Zhang, Yimen Zhang and Xiaoyan Tang, A Method for Nondestructive Measurement of 4H-SiC Epitaxial Layer Thickness Using Stacking Faults, Xi'an: Xidian University, 2010.

[3] Huaqiao Zhao. Research on Key Issues of Full-Spectrum Solar Rectenna, Wuhan: Wuhan University, 2020.

[4] Jun Zhu, Wenqing Liu, Jianguo Liu, Yihuai Lu, Minguang Gao and Liang Xu, Quantitative Analysis of Gases by Fourier Transform Infrared Spectroscopy, Chinese Journal of Scientific Instrument 28(1) (2007), 80-84.

[5] Jiakui Tang, Yong Xue, Tong Yu, Yanning Guan, Guoyin Cai and Yincui Hu, MODIS Land Aerosol Remote Sensing Retrieval: Synergistic Retrieval Algorithm Using TERRA and AQUA MODIS Data, Science in China (Series D: Earth Sciences) 35(05) (2005), 474-481.

[6] Weiwei Feng, Lihuang Lin and Ligang Chen, Study on Polarization Interference Spectrum of Quartz Waveplate, Acta Optica Sinica 27(6) (2007), 1044-1048.

[7] Yandong Zhang, Iterative Least Squares Method for Linear-Nonlinear Model Inversion, Wuhan: Wuhan University, 2018.

[8] Jinrui Yang. Porous Silicon Ethanol Sensor Based on Fabry-Perot Interference Effect, Chongqing: Chongqing University, 2009.

■